Centrifugal instabilities in a curved rectangular duct of small aspect ratio

G. Gauthier,[a] P. Gondret, H. Thomé, and M. Rabaud
Laboratoire Fluides Automatique et Systèmes Thermiques (CNRS UMR 7608, Universités Paris 6 et 11), Bât 502, Campus Universitaire, F-91405 Orsay Cedex, France

(Received 26 July 2000; accepted 25 June 2001)

We report experimental results on the stability of the flow occurring in a curved rectangular duct of small aspect ratio, where the centrifugational forces act along the largest dimension. The basic flow is three-dimensional as in a square or circular curved duct, and above a critical flow rate, streamwise vortices are observed. The threshold of the instability is found to be controlled by a Dean number.
 [DOI: 10.1063/1.1400136]

Centrifugal forces are very efficient mechanism to destablize flows. Among generic cases one can cite the Dean flow between two curved walls close to each other, the Taylor–Couette flow between two rotating cylinders and the Görtler flow over a concave wall.[1] In all these cases, the geometry is infinite in one direction perpendicular to centrifugal forces, and the basic flow is two-dimensional. As the flow parameter (ratio of inertial and centrifugational forces to viscous forces) is increased, the first destabilization leads to a three-dimensional flow consisting of streamwise parallel contrarotating vortices stacked along the curved wall.[1] Since the first theoretical work of Dean, flows in curved ducts of finite aspect ratio (from large values to unity like square ducts or circular pipes) have been the subject of many studies, either theoretical, numerical, or experimental. For aspect ratio of the order of one the basic flow is already three-dimensional and consists of two symmetric counter-rotating vortices,[2,3] the instability leading to a four cell flow.[4] Despite the impressive quantity of studies, to our knowledge only the study of Humphrey *et al.*[5] concerns the case of small aspect ratio, where centrifugal forces act in the direction of the largest dimension. However this study only deals with aspect ratio from 3 to 1/3 and only describes the structure of the basic flow for large radius of curvature. The purpose of this experimental paper is to present first results on the structure and stability of the flow in a rectangular curved channel of small aspect ratio from (1/3 to 1/40), where the width (radial extension) is large compared to the thickness (axial extension) of the cell.

The experimental cell (Fig. 1) consists of two parallel Plexiglass plates separated by two rubber wedges delimiting a ''U''-shaped channel of thickness h and constant width $W=R_2-R_1$, where R_1 and R_2 are, respectively, the inner and outer radius of the curved part. The thickness h of the cell is adjustable in the range 2–10 mm with different sets of rubber wedges, as well as the inner and outer radius R_1 and $R_2(R_1<R_2)$ in the range 25–75 mm and 40–105 mm, respectively. As we are interested in the study of centrifugal instabilities occurring in the curved part of the channel, we will use in the curve the cylindrical coordinates (r,θ,z) corresponding to spanwise, streamwise and normal directions, with $\theta=0°$ at the beginning of the curve. The fluid (water) is injected at the entrance of a first straight section of length $l=20$ cm and jets out at the end of a second one, after a travel along the 180° curved part of the channel. The flow is driven by a constant pressure difference between inlet and outlet. The system is controlled by five dimensional parameters: The volume flow rate Q, the kinematic viscosity ν, the cell thickness h and the radii of curvature R_1 and R_2. One can thus define three independent dimensionless parameters: the aspect ratio $\Gamma=h/(R_2-R_1)$, the curvature $C=(R_2-R_1)/(R_2+R_1)$, and either the Reynolds number $\mathrm{Re}=\overline{U}h/\nu$ built on the cell thickness h and the mean velocity $\overline{U}=Q/h(R_2-R_1)$ or the Dean number $\mathrm{De}=\mathrm{Re}\sqrt{C}$ defined as usually,[1] except that the Reynolds number is here built with h and not with R_2-R_1. In order to visualize the flow we seed water with flakes (5% in volume of Kalliroscope[6]). We explore the flow structure from above or within the gap thickness with two different optical arrangements. The first one is an extended halogen lamp together with a CCD camera perpendicular to the plate. The second one is a laser sheet (helium–neon laser diode) normal to the plate and the main flow direction with a camera located upstream (or downstream) at 45° (along the bisector of the laser sheet and the cell).

The flow in our set-up can be decomposed in three parts, each with its own entry length. In the inflow straight part, the fully developed flow velocity profile is parabolic (Poiseuille like) in the smallest dimension (z) and flat in the largest dimension, except near the corners where exists a viscous boundary layer corresponding to the cell thickness.[7] The entry length for this flow to be fully developed is well known and in our case always smaller than l. In the curved part, there is no theoretical prediction for the ''entry'' angle after which the flow is fully developed but apparently this angle can be large (typically 90° to 180°).[8] However, we know that the fully developed flow will be the classical two-cell one,[2,3] which consists of a centrifugal flow at midway and two centripetal boundary layers near the top and bottom walls. In the present set-up the existence of such a two-roll cell has been checked qualitatively by ink injection as well as by laser sheet visualization. Indeed, from radial laser sheet visualiza-

[a]Present address: Laboratoire de Mécanique de Lille URA 1441, Bât M6, Cité Scientifique, 59655 Villeneuve d'Ascq Cedex. Electronic mail: gauthier@cri.univ-lille1.fr

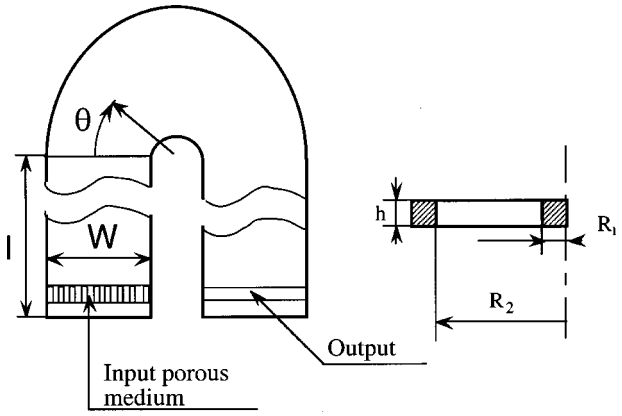

FIG. 1. Experimental set-up. $l=20$ cm, $W=R_1-R_2$ and h, R_1, and R_2 have been varied in the range: $2<h<10$ mm, $25<R_1<75$ mm, and $40<R_2<105$ mm.

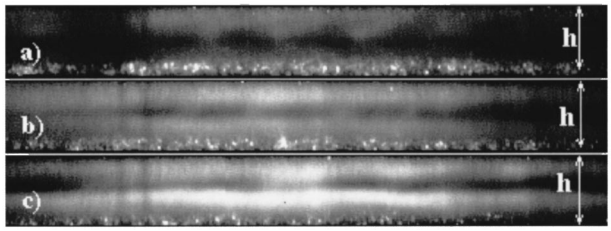

FIG. 2. Laser sheet visualization from upstream for $h=5$ mm, $R_1=25$ mm, and $R_2=104$ mm, and Re=193. Evolution of the flow at (a) $\theta=0°$, (b) $\theta=50°$, and (c) $\theta=90°$. The images show the whole gap of the cell but only the radial extension between $r=40$ mm (to the right) and $r=80$ mm (to the left). The black domains correspond to the walls and the pictures have been corrected from the 45° geometrical deformation.

tion, one can observe the evolution of the flow structure in the thickness of the cell. Figure 2 presents such visualizations for constant flow rate (Re=193) but at increasing orthoradial location θ. In Fig. 2(a), corresponding to $\theta=0°$, the reflected light is not contrasted and almost uniform (note the bright line at the bottom wall due to settled particles). Figures 2(b) ($\theta=50°$) and 2(c) ($\theta=90°$) present both the same structure. It consists of two bright strips close to the upper and bottom walls and a dark line at midway. It had been shown that these bright lines correspond to the limits of the boundary layers.[9] They are brighter in Fig. 2(c) ($\theta=90°$) than in Fig. 2(b) but keep the same location, meaning that the shear is stronger but the boundary layers keep the same thickness. In the outflow straight part, after the curved part, the flow returns to a parabolic profile flow. When these three basic flow structures are observed from above, the reflected light is uniform as shown in Fig. 3(a).

Increasing the flow rate by small incremental values ($\Delta Q=25$ cm^3/s) we observe above a well defined flow rate

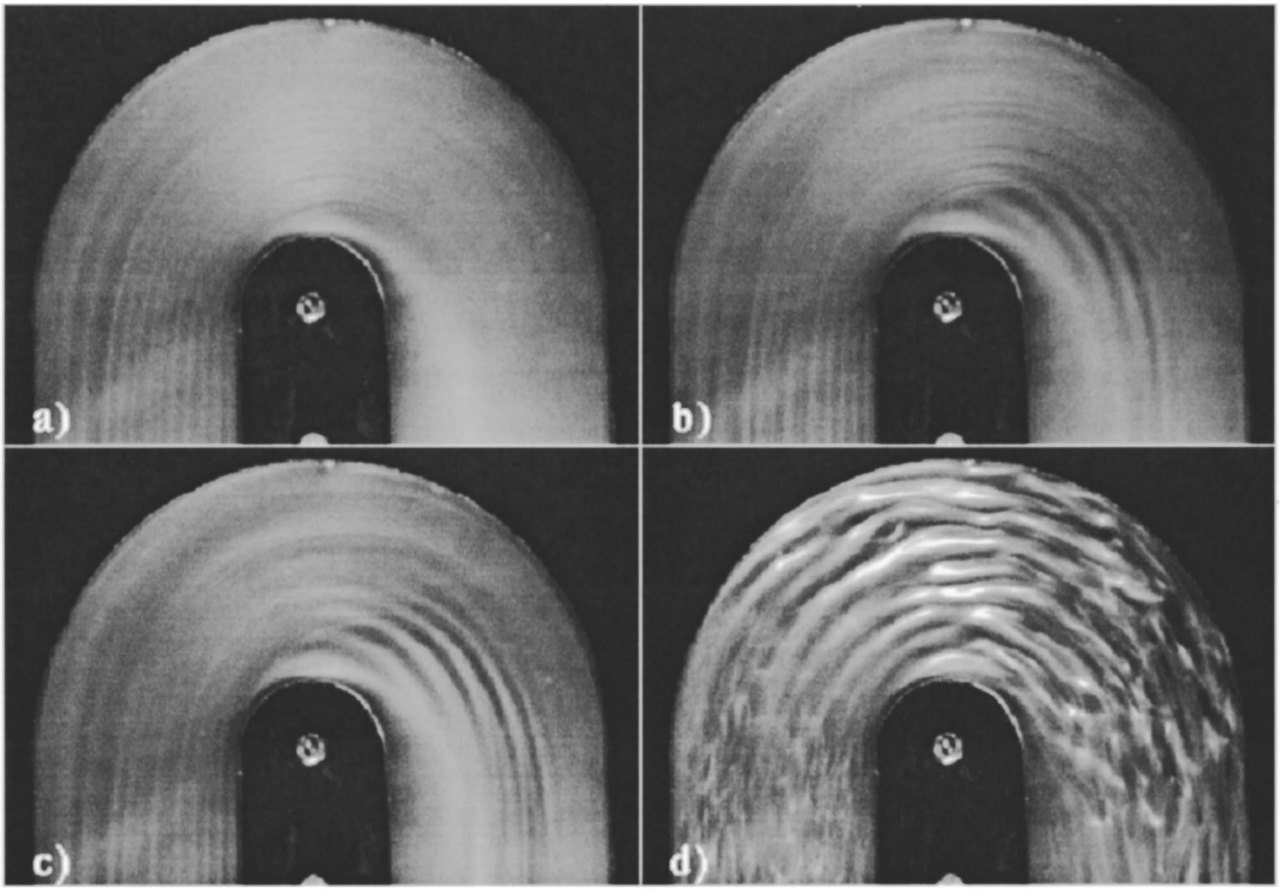

FIG. 3. Different patterns observed from above (for $h=5$ mm, $R_1=25$ mm, and $R_2=105$ mm) at increasing flow rates: (a) Re=62, (b) Re=130, (c) Re=172, and (d) Re=340. The flow is clockwise. Note that some streaks are visible at the bottom left of each figure; they are not related to any instability but to structures created by straws at inlet. These structures are damped but remain visible as fossil streaks.

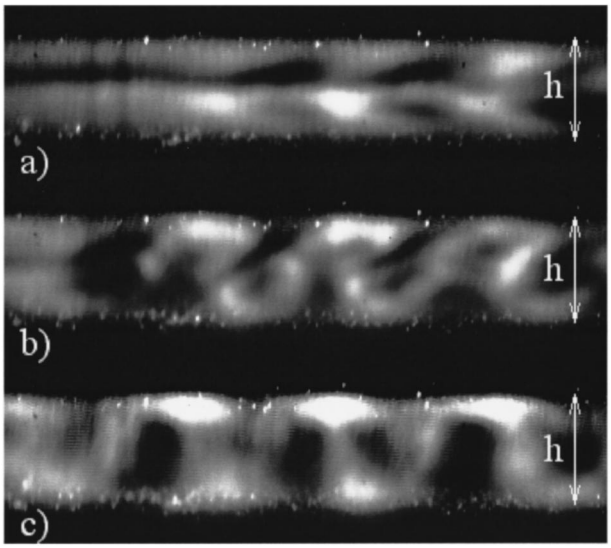

FIG. 4. Evolution of the flow structure in the thickness of the cell, observed at $\theta=135°$ from upstream at increasing flow rates: (a) Re=183, (b) Re =227, and (c) Re=277 ($h=5$ mm, $R_1=25$ mm, and $R_2=105$ mm). The image shows a part of the radial extension of the cell: The right edge corresponds to $r=40$ mm and the left edge to $r=80$ mm. Figure 4(c) looks unfocused as it is a time average of nonstationary structures.

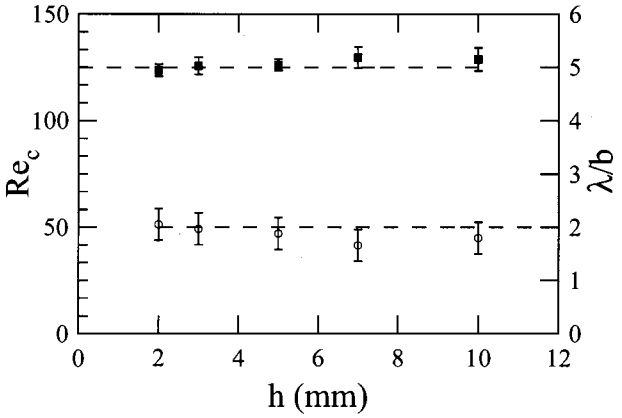

FIG. 5. Evolution with the cell thickness h of the critical Reynolds number Re_c (left and ■) and the dimensionless wavelength λ/h (right and ○). Here $R_1=25$ mm and $R_2=105$ mm.

Q_c, a stationary modulation of the reflected light. At $Q_c-\Delta Q$ nothing is visible, when at Q_c visualization reveals a single stationary vortex extending from $\theta\approx120°$ to the end of the curve and located close to the inner wall. We then defined the onset of the instability as this critical flow rate Q_c. The radial location of this vortex decreases slowly downstream, following an inward spiral. When increasing the flow rate the number of vortices and thus of spiral arms increases and one can observe four spirals in Fig. 3(c). Laser sheet visualizations of Fig. 4 present the evolution of the flow within the cell thickness at $\theta=135°$ for increasing flow rate. Figure 4(a) shows that the instability leads to a radial modulation of each bright strip corresponding to the radial shear zone; this modulation appears first in phase. When the flow rate is further increased, two layers of vortices of increasing intensity are visible in Fig. 4(b), staggered as in the von Karman vortex street. Because of the radial basic flow, they are clockwise in the upper layer and anticlockwise in the lower one. This is confirmed by the fact that they appear different in the upper and lower layers. From above, only the vortices of the upper layer are visible. Still increasing the flow rate, Fig. 4(c) shows that the structures fill now the whole gap and appears as one layer of contrarotating vortices, their center being almost on the same line. Images taken from either sides of the laser sheet (at 45° from upstream or downstream) are shifted by one half wavelength. This behavior is similar to the one observed in the Taylor–Couette flow with the same visualization technique and confirms the contrarotative nature of the vortices.[9] The vortex rearrangement observed between Figs. 4(b) and 4(c) explain the splitting observed from above, e.g., in Fig. 3(c) where each vortices seem to split into two vortices at an angle $\theta_s\approx180°$. The corresponding splitting angle increases with the radial position of the considered spiral and decreases when the flow rate increases. Above a second critical flow rate, peripheral structures undergo an oscillatory instability: they oscillate in the radial direction. This oscillation mode looks very similar to the "wavy mode" observed in the Taylor–Couette flow[1] and though all structures oscillate in phase, they do not present a well selected frequency and the system seems to act as a noise amplifier. The amplitude of the oscillation increases with the radial position. Still increasing the flow rate, the structures progressively becomes more disordered and the flow turns to turbulence [Fig. 3(d)]. The persistence of structures observed far downstream in the outflow straight part is probably due to the stretching of the vorticity caused by the evolution of the mean profile that oppose the diffusing effect of the viscosity.

We have studied the influence on the instability of the three geometrical parameters h, R_1, and R_2 in order to justify *a posteriori* the choice of the dimensionless parameters Γ, C, and Re (or De). Figure 5 shows the influence of the thickness h both on the critical Reynolds number of transition from the uniform flow to the stationary vortex mode and on the wavelength of the structure. The critical Reynolds number $\mathrm{Re}_c=U_ch/\nu$ corresponds to the first visible structure in the set-up and is almost independent of h and equal to 125 ± 5. This confirms that h is the good characteristic length for building the Reynolds number. Measurements of the

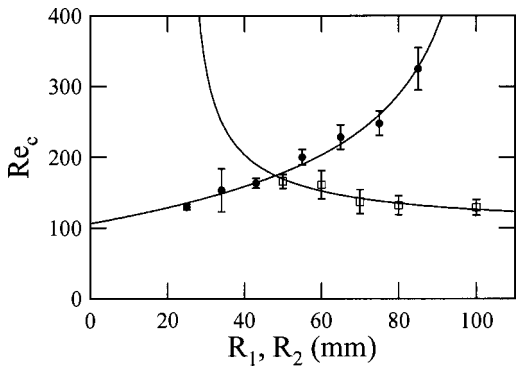

FIG. 6. Critical Reynolds number Re_c versus the inner radius R_1(●) (the outer radius being constant $R_2=105$ mm), and versus the outer radius (□) (the inner radius being constant $R_1=25$ mm). Here $h=5$ mm. The continuous lines correspond in each case to $\mathrm{Re}=100\ \mathrm{C}^{-1/2}$.

wavelength obtained at different flow rates either by laser sheet or by visualization from above are in agreement with the law $\lambda \approx 2 \times h$. On the other hand the influence of each radius of curvature R_1 and R_2 has been investigated separately. Figure 6 shows that variations of R_1 or R_2 have both strong influence on the critical Reynolds number: Re_c increases with R_1 at constant R_2 and decreases with R_2 at constant R_1. A good fit of the experimental points of Fig. 6 corresponds to $\mathrm{Re}_c = 100\ \mathrm{C}^{-1/2}$. This law leads to a constant critical Dean number $\mathrm{De}_c = (U_c h/\nu)\sqrt{(R_2 - R_1)/(R_2 + R_1)} \approx 100$ for the transition to the stationary vortex flow. This result shows that our definition for the Dean number in small aspect ratio cell is pertinent and that the classical definition used in large aspect ratio cell where $(R_2 - R_1)$ replaces h would not work here.

In conclusion experimental results for the centrifugal instability occurring in a curved rectangular duct of small aspect ratio are reported. The instability generates stationary contra-rotating streamwise vortices, which fill the whole thickness of the channel and develop above threshold along both the radial and the azimuthal directions. As far as the onset of the primary instability is concerned, the flow transition is well described by a critical value of a Dean number when geometrical and fluid parameters are modified. However, spatial evolution of the flow above threshold cannot be scaled with the Dean number either for the radial evolution (number of structures) as well as for the downstream evolution (splitting) and new parameter remain to be found.

[1] P. G. Drazin and W. H. Reid, *Hydrodynamic Stability* (Cambridge University Press, Cambridge, 1981).
[2] S. A. Berger, L. Talbot, and L. S. Yao, "Flow in curved pipes," Annu. Rev. Fluid Mech. **15**, 461 (1983).
[3] K. H. Winters, "A bifurcation study of laminar flow in a curved tube of rectangular cross section," J. Fluid Mech. **180**, 343 (1987).
[4] P. A. J. Mees, K. Nandakumar, and J. H. Masliyah, "Instability and transitions of flow in a curved square duct: the development of two pairs of Dean vortices," J. Fluid Mech. **314**, 227 (1996).
[5] J. A. C. Humphrey, A. M. K. Taylor, and J. H. Whitelaw, "Laminar flow in a square duct of strong curvature," J. Fluid Mech. **83**, 509 (1977).
[6] Kalliroscope Corporation, Groton, MA 01450.
[7] P. Gondret, N. Rakotomalala, M. Rabaud, D. Salin, and P. Watzky, "Viscous parallel flows in finite aspect ratio Hele–Shaw cell: Analytical and numerical results," Phys. Fluids **9**, 1841 (1997).
[8] D. E. Olson and B. Snyder, "The upstream scale of flow development in curved circular pipes," J. Fluid Mech. **150**, 139 (1985).
[9] G. Gauthier, P. Gondret, and M. Rabaud, "Motion of anisotropic particles: Application to visualization of three-dimensional flows," Phys. Fluids **10**, 2147 (1998).